A&A 491, L13–L16 (2008)
DOI: 10.1051/0004-6361:200810490

Astronomy & Astrophysics

Letter to the Editor

The redshifted network contrast of transition region emission

W. Curdt[1], H. Tian[1,2], B. N. Dwivedi[1,3], and E. Marsch[1]

[1] Max-Planck-Institut für Sonnensystemforschung (MPS), Max-Planck-Str. 2, 37191 Katlenburg-Lindau, Germany
e-mail: curdt@mps.mpg.de
[2] School of Earth and Space Sciences, Peking University, PR China
[3] Department of Applied Physics, Institute of Technology, Banaras Hindu University, Varanasi-221005, India

Received 1 July 2008 / Accepted 1 October 2008

ABSTRACT

Aims. We study the VUV emission of the quiet Sun and the net redshift of transition region lines in the SUMER spectral range. We aim at establishing a link with atmospheric processes and interpreting the observed downflow as the most evident part of the prevailing global coronal mass transport.
Methods. We rank and arrange all pixels of a monochromatic raster scan by radiance and define equally-sized bins of bright, faint, and medium-bright pixels. Comparing the bright pixels with the faint pixels, we determine the spectrally-resolved network contrast for 19 emission lines. We then compare the contrast centroids of these lines with the position of the line itself. We establish a relationship between the observed redshift of the network contrast with the line formation temperature.
Results. We find that the network contrast is offset in wavelength compared to the emission line itself. This offset, if interpreted as redshift, peaks at middle transition region temperatures and is 10 times higher than the previously reported net redshift of transition region emission lines. We demonstrate that the brighter pixels are more redshifted, causing both a significant shift of the network contrast profile and the well-known net redshift. We show that this effect can be reconstructed from the radiance distribution. This result is compatible with loop models, which assume downflows near both footpoints.

Key words. Sun: UV radiation – Sun: transition region – line: formation – line: profiles

1. Introduction

Observations and interpretations of red- and/or blueshifted emission lines from cosmic objects are crucial to understand the physical processes at work there. The net redshift in the solar transition region (TR) emission lines has been known since the Skylab era (e.g., Doschek et al. 1976, and references therein). Redshifts have also been recorded in stellar spectra (Ayres et al. 1983; Wood et al. 1996). More recently, Brekke et al. (1997) and Chae et al. (1998) independently verified this result, analysing high spectral resolution observations from the Solar Ultraviolet Measurements of Emitted Radiation (SUMER) instrument on *SoHO* (Wilhelm et al. 1995). Both these groups found similar results for the quantitative dependence of the net redshift on line formation temperature in the range from 10^4 K to 10^6 K. The reported peak downflow of 6 to 8 km s^{-1} at a temperature of around 10^5 K is four times higher than the detection limit of the instrument. However, both groups adopted incorrect literature values for the rest wavelengths for the Ne VIII and Mg X emission. Dammasch et al. (1999) and Peter & Judge (1999) have established more realistic rest wavelength values for these species and have demonstrated the disappearance of the net redshift in coronal emission lines. To our knowledge, a satisfactory physical explanation of the net redshift has not yet been found. Peter (2006) has recently reported the first full-Sun VUV emission line profile, showing enhanced emission in the wings.

We present a new method to investigate and explain the TR redshift using the network contrast. A spectrally resolved contrast curve has been included in the SUMER disk atlas of Curdt et al. (2001, hereafter referred to as SDA). Here, the network contrast – defined as the radiance ratio of pixels in the bright network and pixels in the cell interior – has values of about 3 in the continua, and rises to values of 6 to 8 in TR emission lines. A similar result was reported by Reeves (1976). In coronal lines such as Ne VIII and Mg X the contrast is below the background value, a finding which is equivalent to the result of Doschek (2006), who reported a low correlation between the emission of the TR and corona.

An enlarged cutout of the SDA quiet-Sun profile – dominated by the strong Ne VIII, S V, and O IV emission lines around 785 Å – is displayed in Fig. 1. It is also obvious, although not explicitly mentioned in the SDA, that the network profiles are redshifted compared to the emission lines themselves. Our goal is to give a physical explanation for this offset.

In this paper, we extend the earlier work of Reeves (1976) and the work reported in the SDA by a comprehensive investigation of the contrast employing a much larger data set. We show that our result is a direct consequence of the redshift-to-brightness relationship and can be reconstructed by a simple model using multi-component contributions to the line profile. A full discussion of the implications for loop models is beyond the scope of this work. We only present here some salient features, and a detailed study taking account of atmospheric models will be covered in a separate paper.

In contrast to the earlier work of Brekke et al. (1997) and Chae et al. (1998), our new indirect method is unique in several ways, namely:

(i) it does not require an accurate wavelength calibration;
(ii) it is independent of an exact knowledge of the rest wavelength;
(iii) it closely relies on physical processes in the solar atmosphere.

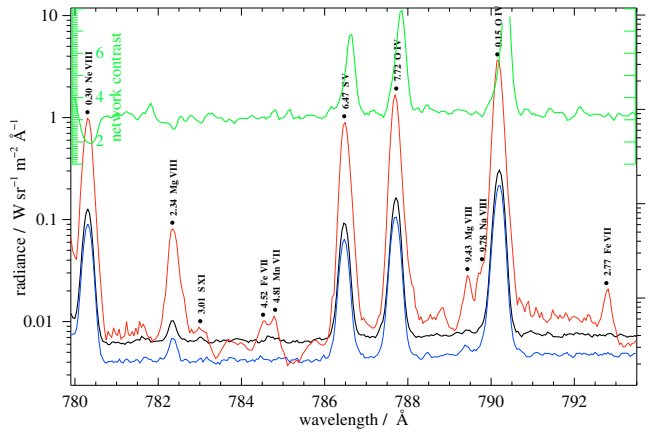

Fig. 1. Enlarged portion of the SUMER spectral atlas (Curdt et al. 2001) showing radiances of average QS (black), sunspot (red), and coronal hole (blue) regions. The network contrast (ratio bright network / cell interior in green), which is normally around 3, increases to values of 6 to 8 in TR lines, and the centroids of the contrast profiles are clearly redshifted.

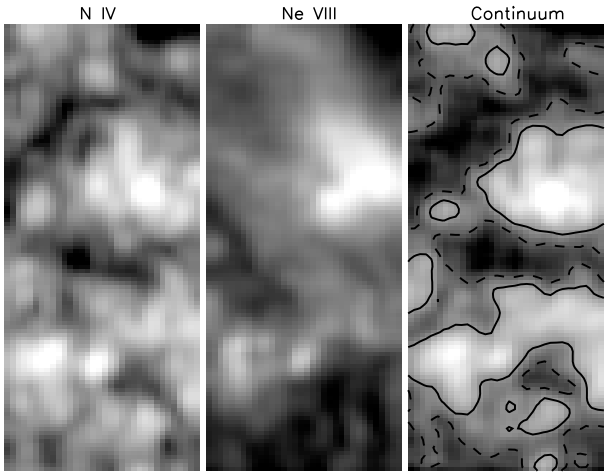

Fig. 2. Raster scan in the emission of N IV, Ne VIII and the continuum around 780 Å. In the continuum map brightness contours at 33% and 67% levels are overlaid. These have been used to define bright, faint and medium-bright pixels.

2. Method

The signal in each pixel is a mixture of emission from different plasmas along the LOS and from unresolved fine structures. We have decomposed them by a statistical method based on the assumption that statistically different components can be separated in the radiance distribution. In our new method, we differentiate among different classes of brightness in the radiance distribution instead of simply averaging the brightness over all pixels. We assume that individual bins of different brightness do behave differently. In particular, we make use of the fact that brighter pixels have a tendency to appear redshifted in many emission lines. Such a redshift-to-brightness relationship was also noted by Dammasch et al. (2008) in a different data set, and must consequently have an imprint on the network contrast. This is the core of our method: the strong redshift observed in the network contrast as compared to the position of the line itself. For a collection of prominent, blend-free emission lines, we determined the network contrast (ratio of 33% of the brighter pixels as compared to 33% of the dim pixels) and compared the contrast curve to the emission line itself.

A rather crude and empirical method was used in the SDA to display the network contrast; the radiance of a few bright pixels out of 300 along the slit, which were thought to represent the network, was compared to the radiance of the remaining pixels. The pixel selection was made in a static way for all 36 individual exposures of the data set, a procedure that may not be appropriate in view of the temporal evolution of the Sun. However, the shift of the slit image caused by the wavelength scan (due to misalignment of the grating) had been compensated for by employing the standard delta_pixel routine.

In the present analysis, we measure and compare the position of the line centroids (the line center determined by spectral centroiding) relative to the position of the contrast maximum or minimum. We find that the centroid of the contrast profile is normally shifted by several pixels towards longer wavelengths.

3. Observations

The data set in the SDA is a snapshot of 300 pixels along the slit. Thus, the given spectral radiances still have significant uncertainties and can only approximately represent the quiet Sun. Also, better values for the network contrast could have been achieved if a better statistical basis were available like the one we report here, where rasters are observed instead of a single exposure. Our data set consists of raster scans of size $51'' \times 120''$ in 14 different wavelength windows of ≈44 Å covering the entire wavelength range from 670 Å to 1490 Å with only few insignificant gaps. We employed a slit of size $1'' \times 120''$. The raster increment was $1.5''$ and the exposure time was 90 s. The rasters were obtained in the so-called 'Schmierschritt' mode, which means that each transmitted spectrum is composed of four elementary exposures with a 22.5 s dwell time and a $0.375''$ step increment (Wilhelm et al. 1995). We already compensated on board for the parasitic movement of the slit image mentioned earlier. Therefore, we can safely assume that the North-South offset between the individual rasters is negligible. We have compensated for the solar rotation after each raster scan. Therefore, we also assume that all rasters do map the same portion of the Sun in the East-West direction.

Our data set was obtained during an observation on 5 April 2007 running from 00:51 UTC to 13:10 UTC. The initial pointing – centre of the first raster – was $x = 0$, $y = 0$. Fifty minutes are needed for each raster. Standard procedures from the SUMERsoft library[1] were applied for the data reduction.

The major improvement of this observation (called the "super atlas") as compared to a normal reference spectrum is the increase of the number of pixels by more than an order of magnitude. This data set allows us to produce monochromatic raster scans for all emission lines and all continua in the SUMER spectral range. As an example, we show in Fig. 2 the maps obtained simultaneously in the emission of N IV, Ne VIII and in the continuum around 780 Å.

We have selected 19 prominent and blend-free emission lines to produce monochromatic maps. For each raster we also produce a map of the continuum. We use this continuum map, where the elements of the chromospheric network are well-structured and at instrument resolution, to rank all pixels by radiance. We define equally-sized bins of bright network pixels, of faint

[1] SUMERsoft is a software library, which constitutes the integrated experience with SUMER data analysis tools. It is available at http://www.mps.mpg.de/projects/soho/sumer/text/list_sumer_soft.htm

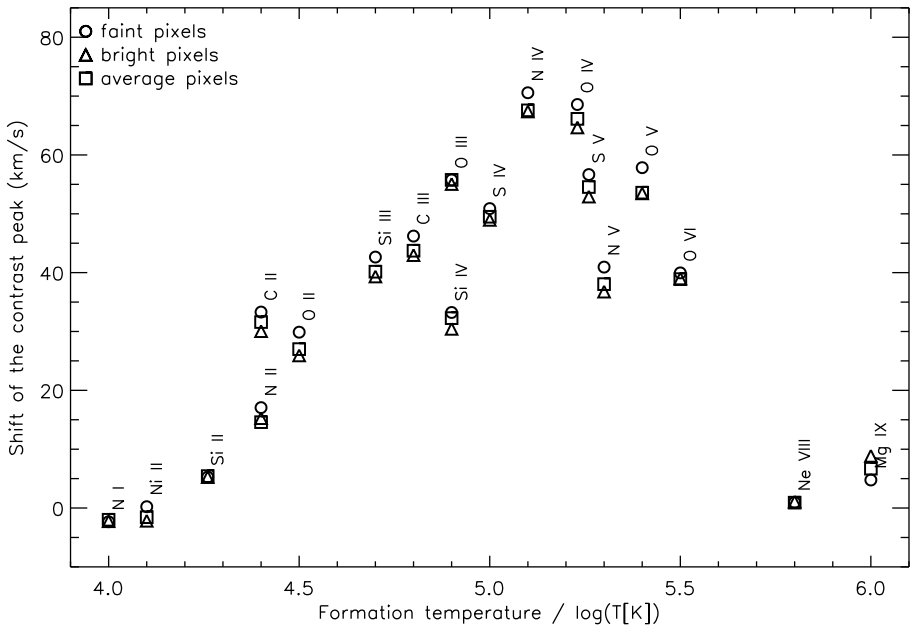

Fig. 3. The shift of the network contrast relative to the position of the emission line as a function of formation temperature. Individual offsets have been determined for comparison with the profile of the bright pixels (△), the faint pixels (○), and the average pixels (□). The shift is scaled as Doppler flow. This is to make it comparable to earlier, direct measurements and should not be confused with a real flow.

Table 1. Observed offset of the network contrast for 19 emission lines. Lines from the same raster are co-temporal, raster start and stop time are in UTC.

Line	λ / Å	log T/K	$\Delta\lambda$ / Å	Time
Mg IX	749.54	6.0	0.017	01:44–02:35
S IV	750.22	5.0	0.124	01:44–02:35
N IV	765.15	5.1	0.172	02:37–03:28
Ne VIII	780.30	5.8	0.002	02:37–03:28
S V	786.47	5.26	0.143	02:37–03:28
O IV	787.72	5.23	0.174	02:37–03:28
O V	761.99	5.4	0.136	02:37–03:28
O II	833.32	4.5	0.075	03:30–04:20
O III	833.74	4.9	0.155	03:30–04:20
C III	977.03	4.8	0.142	05:15–06:06
C II	1037.00	4.4	0.109	06:08–06:59
O VI	1031.93	5.5	0.134	06:08–06:59
N II	1083.99	4.4	0.053	07:01–07:52
Si III	1206.51	4.7	0.161	07:54–08:45
N V	1238.82	5.3	0.157	08:48–09:39
Si II	1309.28	4.26	0.024	10:33–11:24
Ni II	1317.22	4.1	–0.007	10:33–11:24
N I	1318.98	4.0	–0.009	10:33–11:24
Si IV	1402.77	4.9	0.151	11:26–12:17

cell-interior pixels and of pixels with medium brightness. The same bin definition was used for all emission lines in a raster for the determination of the spectrally resolved contrast profile. For each spectral pixel the ratio of the radiance found in the bright-pixel bin over that of the faint pixel bin was determined. Like in the SDA, a significant increase of the contrast is observed for all lines except for N I, Ni II, Si II, Ne VIII, and Mg IX, which show a contrast minimum. To account for temporal variations, we have repeated the definition of radiance bins for each raster.

All selected lines are listed in Table 1 with wavelength and formation temperature and with the offset results and timing information of the relevant raster. In order to compare our result with previous work, we have converted the offsets to Doppler flows, applying $v/c = \Delta\lambda/\lambda$. Figure 3 displays the main result of our work.

Individual offsets have been determined for a comparison with the profile of the bright pixels (△), the faint pixels (○), and the average pixels (□). In TR emission, the data points for the bright and for the faint pixel profiles deviate, as can be expected from the earlier work of Brekke et al. (1997) and Chae et al. (1998). This interesting secondary result is a direct consequence of the redshift-to-brightness relationship.

4. Discussion and summary

Figure 3 has similarities to the respective figures in Brekke et al. (1997) and Chae et al. (1998). We have expressed the offset $\Delta\lambda$ in speed units of Doppler flow and arrived at values of about 60 km s^{-1}. This is about 10 times higher than the average net downflow found in earlier work. This finding demonstrates that our new method enhances the visibility of the Doppler shift, which leads to a significant increase of the sensitivity, but should not be confused with a real flow.

We now use a simple model to reconstruct the observed redshift of the network contrast. We use the fact that the radiance distribution of the average quiet Sun follows a single lognormal distribution function and that a redshift-to-brightness relationship exists. Pauluhn et al. (2000) have shown in great detail that the emission of the quiet Sun including the network and the internetwork is better described by a lognormal distribution than by two Gaussians. This is in agreement with the brightness distribution of the λ765 N IV TR line, as shown in Fig. 4a.

For this distribution, we have defined 40 equally sized radiance bins. For each bin we determined the line position. We found a linear relationship between the logarithm of the spectral radiance, L_λ, and the redshift of the line centroid, as displayed in Fig. 4b. Dammasch et al. (2008) applied a different bin definition, but they arrive at a similar result of 3 km s^{-1} per radiance decade. We now use the redshift-to-brightness relationship to rescale the abscissa in the histogram in Fig. 4c and define separate groups of bright pixels, of faint pixels and the pixels of medium brightness. The pixels in each group are convolved with a Gaussian line profile typical for TR emission on a continuum background. Thus we arrive at three different profiles for those groups of pixels. As a consequence of the redshift-to-brightness relationship shown in Fig. 4b, the reconstructed profiles are

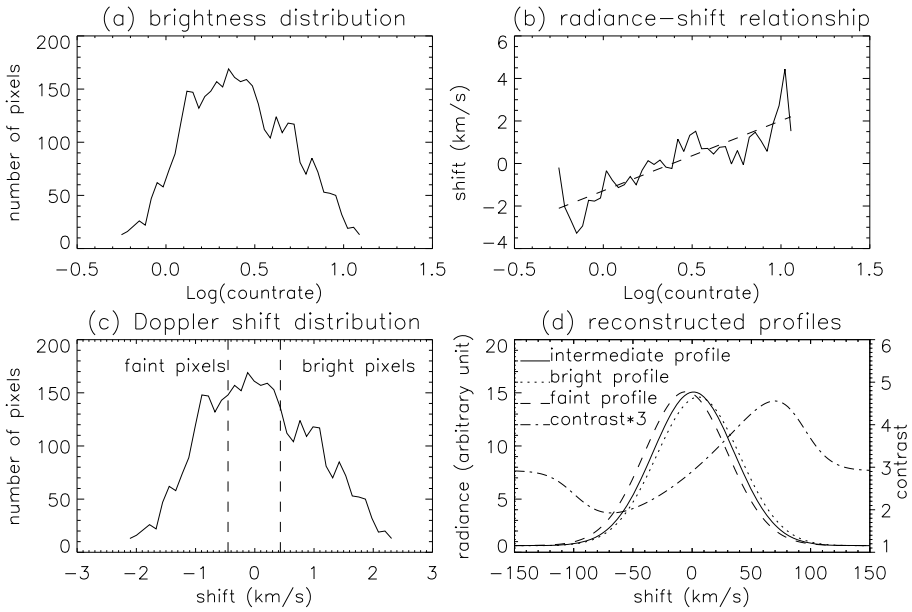

Fig. 4. Reconstruction of the observed network contrast in the radiance of the λ765 N IV TR line **(a)** employing the also observed redshift-to-brightness relationship **(b)** to rescale the abscissa of the lognormal radiance distribution **(c)** and a convolution of three separate groups of pixels with a Gaussian profile on a continuum **(d)**.

offset from each other by a few km/s (cf., Fig. 4d). The contrast profile – the ratio of the bright profile to the faint profile – peaks, however, near a redshift value of ≈70 km s^{-1}, which is close to our empirical result in Fig. 3. This demonstrates that the observed offset of the network contrast can be reconstructed in a quantitative manner with some basic assumptions. We note that the contrast profile, which we use in our new method, is much more sensitive to shifts than the line profile itself. We also note that the observed skewness of the contrast profile in lines like λ780 Ne VIII or λ1032 O VI seems to be a real result of the reconstruction (cf., Fig. 4d).

We emphasize that our results cannot be used to make any statement about systematic flows in coronal emission. The contrast depression simply indicates that the corona is decoupled from the chromosphere, and therefore no deviation from the rest wavelength can be expected for the contrast minimum. Cool plasma with a low degree of ionization will not be guided by the magnetic field and will also not participate in the concentration process in the downflow near loop footpoints. The redshift-to-brightness relationship as a direct consequence of this most evident part of the prevailing global coronal mass transport (Marsch et al. 2008) may be the physical explanation for the well-known net redshift in TR emission and of the offset in the spectrally resolved network contrast.

Our new result corroborates the recent work of Dammasch et al. (2008) and Marsch et al. (2008). In actuality, blueshifts and redshifts respectively correspond to upflows and downflows of the plasma on open and closed field lines as noted by Marsch et al. (2008). The redshifted network contrast of TR emission, ubiquitous redshifts and sporadic blueshifts in the solar atmosphere show the physical characteristics of mass transport which we may term as "coronal convection".

Dammasch et al. (2008) argue that the downflow concentrated near both footpoints of coronal loops is powered by a quasi-continuous heating process. They follow the suggestion of Feldman et al. (2001) and infer that unresolved bright features in the network are tiny loops, which are also redshifted at both legs. Pauluhn & Solanki (2007) developed a heuristic nanoflare model showing that continuous small-scale brightenings could produce the observed radiance distribution. Fontenla et al. (2007, 2008) assume that the Farley-Bunemann instability could be responsible for the heating process. It is difficult to use our observation in favour of or against any nanoflare heating model reported in the literature (see the review of Innes 2004, and references cited therein). These questions can certainly not be answered from our observation alone. More theoretical work is needed, which is beyond the scope of this communication.

Acknowledgements. The SUMER project is financially supported by DLR, CNES, NASA, and the ESA PRODEX Programme (Swiss contribution). SUMER is part of *SOHO* of ESA and NASA. The work of B.N.D. was supported by a grant from the MPS. H.T. is supported by China Scholarship Council for his stay at MPS. We thank the referee for critical comments which improved the clarity of this Letter.

References

Ayres, T. R., Stencel, R. E., Linsky, J. L., et al. 1983, ApJ, 274, 801
Brekke, P., Hassler, D. M., & Wilhelm, K. 1997, Sol. Phys., 175, 349
Chae, J., Yun, H. S., & Poland, A. I. 1998, ApJS, 114, 151
Curdt, W., Brekke, P., Feldman, U., et al. 2001, A&A 375, 591
Dammasch, I. E., Wilhelm, K., Curdt, W., & Hassler, D. M. 1999, A&A, 346, 285
Dammasch, I. E., Curdt, W., Dwivedi, B. N., & Parenti, S. 2008, Ann. Geophys., 26, 2955
Doschek, G. A. 2006, ApJ, 649, 515
Doschek, G. A., Feldman, U., & Bohlin, J. D. 1976, ApJ, 205, L177
Feldman, U., Dammasch, I. E., & Wilhelm, K. 2001, ApJ, 558, 423
Fontenla, J. M., Curdt, W., Avrett, E. H., & Harder, J. 2007, A&A, 468, 695
Fontenla, J. M., Peterson, W. K., & Harder, J. 2008, A&A, 480, 839
Innes, D. E. 2004, in Waves, Oscillations and Small-Scale Transient Events in the Solar Atmosphere: A Joint View from SOHO and TRACE, Proc. SOHO 13, Palma de Mallorca Oct. 2003, ed. H. Lacoste, ESA SP, 547, 215
Marsch, E., Tian, H., Sun, J., Curdt, W., & Wiegelmann, T. 2008, ApJ, 685, 1262
Pauluhn, A., & Solanki, S. K. 2007, A&A, 462, 311
Pauluhn, A., Solanki, S. K., Rüedi, I., Landi, E., & Schühle, U. 2000, A&A, 362, 737
Peter, H. 2006, A&A, 449, 759
Peter, H., & Judge, P. 1999, ApJ, 522, 1148
Reeves, E. M. 1976, Sol. Phys., 46, 53
Wilhelm, K., Curdt, W., Marsch, E., et al. 1995, Sol. Phys., 162, 189
Wood, B. E., Harper, G. M., Linsky, J. L., & Dempsey, R. C. 1996, ApJ, 458, 761